Visible-Light-Induced Degradation of Rhodamine B by Nanosized Bi_2WO_6

Hongbo Fu, Chengshi Pan, Wenqing Yao, and Yongfa Zhu*

Department of Chemistry, Tsinghua University, Beijing 100084, People's Republic of China

Received: June 6, 2005; In Final Form: September 1, 2005

Visible-light-induced photodegradation of rhodamine B over nanosized Bi_2WO_6 has been observed. Bi_2WO_6 exhibited a high photoactivity to photodegrade rhodamine B in the central pH solution under visible irradiation ($\lambda > 420$ nm). After five recycles for the photodegradation of rhodamine B, the catalyst did not exhibit any significant loss of activity, confirming the photocatalyst is essentially stable. The total organic carbon measurement displayed that a high degree of mineralization was achieved in the present photochemical system. The results of density functional theory calculation illuminated that the visible-light absorption band in the Bi_2WO_6 catalyst is attributed to the band transition from the hybrid orbitals of Bi6s and O2p to the W5d orbitals. The Bi_2WO_6-assisted photocatalytic degradation of rhodamine occurs via two competitive processes: a photocatalytic process and a photosensitized process. The transformation of rhodamine is mainly via the photocatalytic process. Kinetic studies by using electron spin resonance and the radical scavenger technologies suggest that •OH is not the dominant photooxidant. Direct hole transfers and $O_2^{\bullet-}$ could take part in Bi_2WO_6 photocatalysis. This study provided a possible treatment approach for organic pollutants by using visible light in aqueous ecosystems.

1. Introduction

Dyes are important organic pollutants, and their release as wastewater in the ecosystem is a dramatic source of esthetic pollution, eutrophication, and perturbations in aquatic life.[1−4] Most the dyes are resistant to biodegradation and direct photolysis, and many N-containing dyes such as rhodamine B (RhB) undergo natural reductive anaerobic degradation to yield potentially carcinogenic aromatic amines.[1] Zhao et al.[5−7] reported that some dyes could be degraded under visible-light irradiation over TiO_2 by a self-photosensitized process. Mechanistically, it is now commonly accepted that the dye is only the light absorbing species.[5] From the excited state of the dye, an electron is injected into the conduction band of TiO_2 where it is captured by the surface adsorbed O_2 to produce $O_2^{\bullet-}$, and then, the dye cation radicals are decomposed subsequently via attack by oxygen active species.[5] However, its photoefficiency is very low due to the much slower interfacial electron transfer to the oxidize sensitizer. Furthermore, no further photoinduced transformation of dye pollutants occurs once the dye is bleached, and the complete mineralization of the dye has not been achieved.[6] Therefore, the development of efficient visible-light-induced photocatalysts for dye photodegradation has been an urgent issue from the viewpoint of using solar energy.

The pioneering works done by Zou et al.[8] displayed water splitting for H_2 and O_2 evolution in a stoichiometric amount over the $NiO_x/In_{0.9}Ni_{0.1}TaO_4$ photocatalyst under visible-light irradiation. Following this work, many new visible-light-driven catalysts have also been reported.[9−12] However, only a few studies have been conducted so far with the aim of environmental treatment of organic pollutants in water.[9,10] In oxide semiconductors, the conduction band levels of small-band-gap semiconductors are usually low because the deep valence bands are formed by O2p. This is a major problem for developing visible-light-driven and stable oxide photocatalysts. To find a breakthrough, it is indispensable to control the valence band with orbitals of some elements instead of O2p. It has been found that bismuth is a potential candidate for such a valence band control element.[13] Recently, a great deal of effort has been devoted to developing photocatalysts containing bismuth with high activities for environmental applications and/or water splitting, such as $BiVO_4$,[14−16] $CaBi_2O_4$,[9] $Bi_2Ti_2O_7$,[17] and $Bi_4Ti_3O_{12}$.[18]

Bi_2WO_6 has been found to possess interesting physical properties such as ferroelectric piezoelectricity, pyroelectricity, catalytic behavior, and a nonlinear dielectric susceptibility.[19] Recently, Kudo and his co-worker[20] demonstrated photocatalytic O_2 evolution by Bi_2WO_6 from $AgNO_3$ solution. More recently, Zou et al.[21] reported that Bi_2WO_6 showed not only the activity for photocatalytic O_2 evolution but also the activity of mineralizing both $CHCl_3$ and CH_3CHO contaminants under visible-light irradiation. Therefore, the photocatalyst with a strong oxidizing potential could be postulated.

Recently, we have reported the formation mechanism of the nanostructured Bi_2WO_6 in the hydrothermal process. The photoactivity of the nanosized Bi_2WO_6 was primarily evaluated.[22] In the present study, the photodegradation of dyes over nanosized Bi_2WO_6 under visible-light irradiation was further studied from mechanistic and kinetic viewpoints. The information on the fate of the valence band hole and the details of the photoreaction mechanism were clarified. The band structure of Bi_2WO_6 was also discussed on the basis of density functional theory (DFT) calculations.

2. Experimental Section

2.1. Materials. Bi_2WO_6 was prepared by hydrothermal synthesis according to our previous report.[22] The spin trap 5,5-dimethyl-1-pyrroline-*N*-oxide (DMPO) was kindly supplied. Particulate TiO_2 (particle diameter 30 nm, surface area 50 m^2 g^{-1}, product name P-25) is commercially available from

* Corresponding author. Phone: (+86)-10-6278-7601. Fax: (+86)-10-6278-7601. E-mail: zhuyf@mail.tsinghua.edu.cn.

10.1021/jp052995j CCC: $30.25
Published on Web 10/21/2005

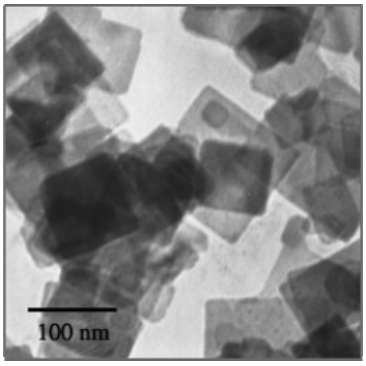

Figure 1. TEM image of the nanosized Bi_2WO_6 prepared by hydrothermal reaction in the present study. $[Bi_6^+]/[WO_4^{2-}] = 1:1$, pH 7.00.

Degussa Corp. and was used as a reference photocatalyst. Other chemicals were all of analytical reagent grade quality and used without further purification. Deionized and doubly distilled water were used throughout this study. RhB, a widely used dye, was chosen as a representative dye pollutant, and the structure of the RhB molecule is illustrated below; the small letters identify the protons for H^1 NMR identification.

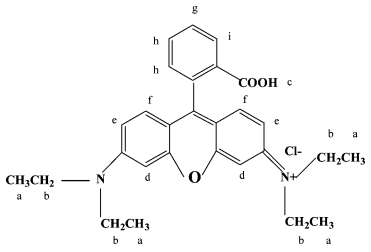

The structure of RhB

2.2. Characterizations. X-ray diffraction (XRD) obtained with a Bruker D8-advance X-ray diffractometer was identical to the standard card (JCPDS 77-1126). The rounding of the baseline spectra indicated the presence of trace amounts of amorphous oxides. Its Brunauer−Emmet−Teller (BET) specific surface area was 43.2 $m^2\ g^{-1}$. A transmission electron microscopy (TEM) study was carried out on a JEM 1010 electron microscopy instrument. The TEM image shown in Figure 1 shows that the Bi_2WO_6 crystals prepared by the hydrothermal process are sheet-shaped. The sizes of the crystals were distributed in the scope from 50−200 nm. UV−visible diffuse reflectance spectra (UV−vis DRS) were obtained by using a Hitachi U-3010 spectrophotometer. $BaSO_4$ was the reference sample, and the spectra were recorded in the range 200−700 nm.

2.3. Photoreactor and Light Source. The visible-light source was a 500 W xenon lamp (Institute of Electric Light Source, Beijing) positioned beside a cylindrical reaction vessel. The system was cooled by wind and maintained the room temperature. An appropriate cutoff filter was placed inside the vessel to ensure complete removal of radiation below 420 nm and to ensure that irradiation of the RhB/Bi_2WO_6 system occurred only by visible-light wavelengths. The average light intensity was 30 mW cm^{-2}.

2.4. Procedure and Analyses. Aqueous suspensions of RhB (usually 100 mL, 1×10^{-5} M) and 50 mg of the Bi_2WO_6 powder were placed in a vessel. Prior to irradiation, the suspensions were magnetically stirred in the dark for ~30 min to ensure the equilibrium of the working solution. At given time intervals, 3 mL aliquots were sampled and centrifuged to remove the particles. The filtrates were analyzed by recording variations of the absorption band maximum (553 nm) in the UV−vis spectra of RhB by using a Hitachi U-3010 UV−vis spectrophotometer. The extent of adsorption of RhB on Bi_2WO_6 was determined by the difference in the concentration of RhB between the original solution and the filtrate of the RhB/Bi_2WO_6 suspensions. In the anaerobic study, the solution was deaerated by bubbling high pure N_2 gas for half an hour in the dark before irradiation. N_2 gas purge was continued during the irradiation.

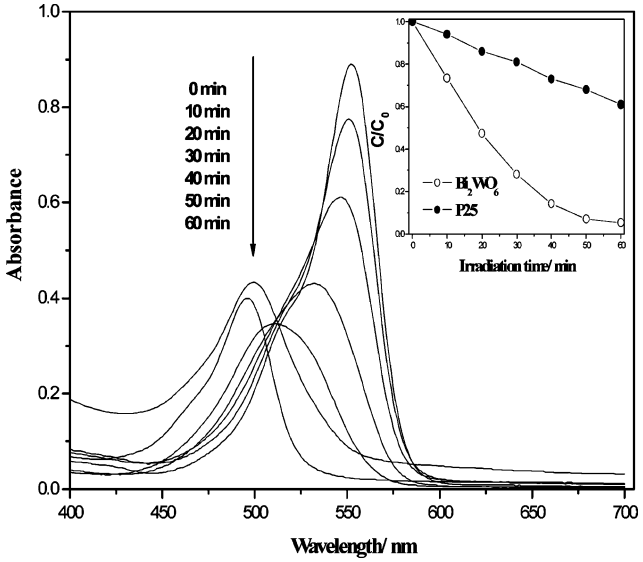

Figure 2. UV−visible spectral changes of RhB (1×10^{-5} M) in aqueous Bi_2WO_6 dispersions as a function of irradiation time. Inset: RhB concentration changes over Bi_2WO_6 and P-25, pH 7.50, $\lambda > 420$.

Electron spin resonance (ESR) signals of radicals spin-trapped by DMPO were recorded at ambient temperature on a Bruker ESR 300 E spectrometer: the irradiation source was a Quanta-Ray Nd:YAG pulsed laser system ($\lambda = 355$ nm, 10 Hz). H^1 NMR spectra were obtained with a Varian 300 nuclear magnetic resonance spectrometer. Samples were prepared as follows: several suspensions containing 200 mL of the RhB dye (2×10^{-4} M) and 200 mg of Bi_2WO_6 were irradiated at different time intervals, following which the Bi_2WO_6 particles were removed by centrifugation as described above. Subsequently, the solvent of the filtrate was removed under reduced pressure (below 323 K). The remaining residue was dissolved in 0.5 mL of D_2O. Total organic carbon (TOC) was measured by a Tekmar Dohrmann Apollo 9000 TOC analyzer. NH_4^+ and NO_3^- ions were analyzed with an ion chromatograph (Shimadzu LC-10AS).

2.4. Electronic Structure Calculation. The quantum-mechanical calculations performed here are based on density functional theory (DFT).[23] Exchange-correlation effects were taken into account by using the generalized gradient approximation (GGA). The total energy code CASTEP was used, which utilizes pseudopotentials to describe electron−ion interactions and represents electronic wave functions using a plane-wave basis set.[24] The kinetic energy cutoff was set at 300 eV.

3. Results and Discussions

3.1. Photodegradation of RhB. The temporal evolution of the spectral changes taking place during the photodegradation of RhB over Bi_2WO_6 was displayed in Figure 2. Tetraethylated rhodamine shows a major absorption band at 553 nm. Visible-light irradiation ($\lambda > 420$ nm) of the aqueous RhB/Bi_2WO_6 dispersion leads to an apparent decrease in absorption with a

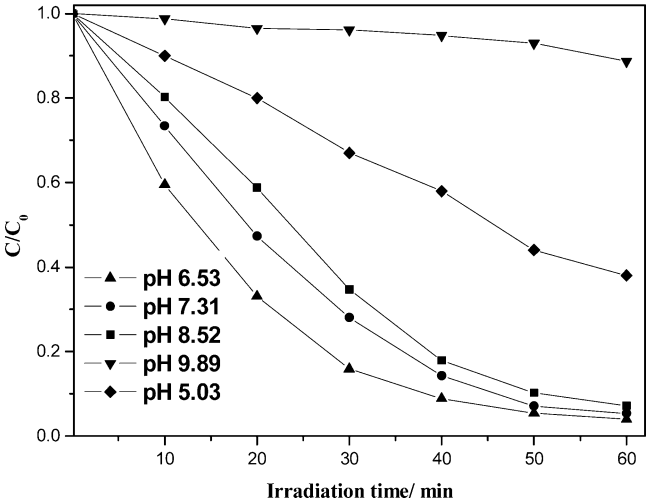

Figure 3. Concentration percent of photocatalytic RhB (1×10^{-5} M) by Bi_2WO_6 (0.5 g L^{-1}) in solution against time of photocatalysis at different pHs; $\lambda > 420$ nm.

concomitant wavelength shift of the band to shorter wavelengths. Under visible illumination, the dye is de-ethylated in a stepwise manner with the color of the dispersion changing from an initial red color to a light green-yellow (i.e., ethyl groups are removed one by one, as confirmed by the gradual peak wavelength shifts toward the blue region). The fully de-ethylated RhB molecule has a major absorption band at $\lambda_{max} = 506$ nm, in accordance with the standard spectra of RhB. The color of the dispersion disappeared (after 90 min of irradiation), indicating that at least the chromophoric structure of the dye was destroyed. Comparison of the spectrum after 60 min of irradiation with the initial one shows that approximately 47.1% of RhB formed rhodamine after being fully demethylated and the rest was degraded through the destruction of the conjugated structure. The inset of Figure 2 showed the temporal concentration changes of RhB. For comparison, the photosensitized degradation of RhB by TiO_2 (P-25) was also performed. One can see that the loss of RhB over Bi_2WO_6 was more rapid than that in the case of P-25.

The photodegradation of RhB over Bi_2WO_6 with different initial pHs is displayed in Figure 3. A variation in pH from 5.03 to 9.89 greatly influences the photoassisted degradation of RhB in aqueous Bi_2WO_6 dispersions. The photodegradation rate of the RhB dye decreased from pH 6.53 to 9.98. However, a drastic decrease of the degradation rate was found at pH 5.03. The highest degradation rate was achieved at pH 6.53. The prevailing pH of the solutions can affect the mode and extent of adsorption of RhB on the Bi_2WO_6 surface and thus, indirectly, the transformation rate of RhB. To further elucidate the relationship between the extent of adsorption and the photodegradation process, we examined the influence of pH on the adsorption of RhB on the catalyst surface, as shown in Figure 4. Clearly, both the adsorption of RhB and the initial rate of RhB conversion decreased with an increase in the pH of the dispersion in the scope of pH 6.53−9.89, suggesting that high adsorption of RhB by Bi_2WO_6 promotes the transformed rate. An exception occurred at pH 5.03; another unknown factor may affect the greatly reduced photocatalytic activity. The solid particles were gained from the acidic suspension (pH 4.70) by a simple filtration and then observed by XRD. For comparison, XRD of the Bi_2WO_6 particles gained from the central solution (pH 7.50) was also measured. The results are shown in Figure 5. Apparently, Bi_2WO_6 was unstable in acidic solution. It could completely transform to H_2WO_4 and Bi_2O_3, which is the reason that Bi_2WO_6 has a poor catalytic activity in acidic solution.

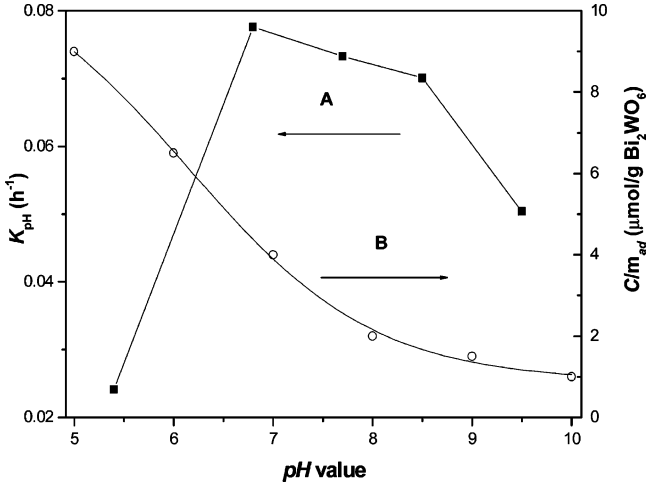

Figure 4. Influence of pH value on the photocatalytic degradation kinetic rate constant of RhB over Bi_2WO_6 (A) and adsorption of RhB on the surface of Bi_2WO_6 (B); Bi_2WO_6 loading, 0.5 g L^{-1}; initial concentration of RhB, 1×10^{-5} M; $\lambda > 420$ nm.

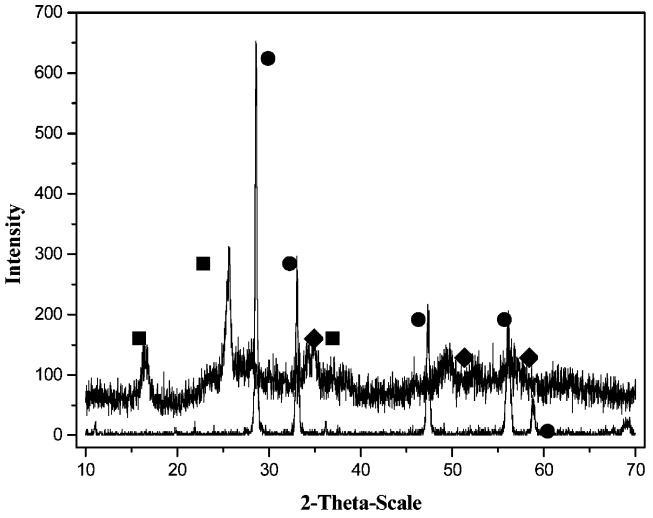

Figure 5. XRD patterns of Bi_2WO_6 at pH 4.70 (upside) and pH 7.50 (downside): Bi_2WO_6 (●), H_2WO_4 (■), Bi_2O_3 (◆).

The influence of the initial RhB concentration (C_0) on the photocatalytic rate was also inspected, and the results are shown in Figure 6. Via changing C_0 in the range 1×10^{-6}−1×10^{-4} M, the plots of irradiation time (t) versus C_0/C exhibited a nearly straight line. The determined reaction rate constant (k) was 0.0714, 0.0592, 0.0517, 0.0218, and 0.0146 min^{-1}, respectively, for initial concentrations of RhB of 1×10^{-6}, 5×10^{-6}, 1×10^{-5}, 5×10^{-5}, and 1×10^{-4} M. It can be seen that the initial concentration of RhB has a significant effect on the degradation rates. The rate of photodegradation of RhB is faster when the initial concentration is lower. The above first-order linear relationship can be explained in the Langmuir−Hinshelwood model

$$r = \frac{-dC}{dt} = -\frac{kKC}{1 + KC} \quad (1)$$

As for the dilute solution, $KC \leq 1$ (K refers to the adsorption equilibrium constant), because of the weak adsorption of RhB on the surface of the catalyst, the above model can be expressed by

$$r = kKC \quad (2)$$

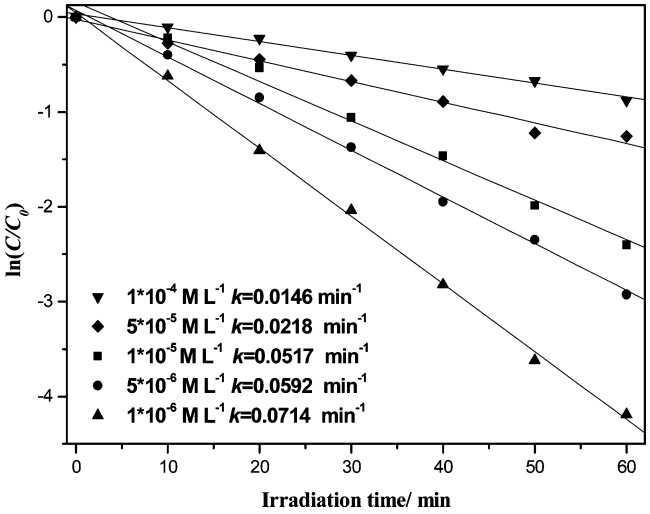

Figure 6. First-order plots for the photocatalytic degradation of RhB by Bi_2WO_6 particles at various initial concentrations; the suspensions containing 0.5 g L^{-1} Bi_2WO_6, pH 7.50, $\lambda > 420$ nm.

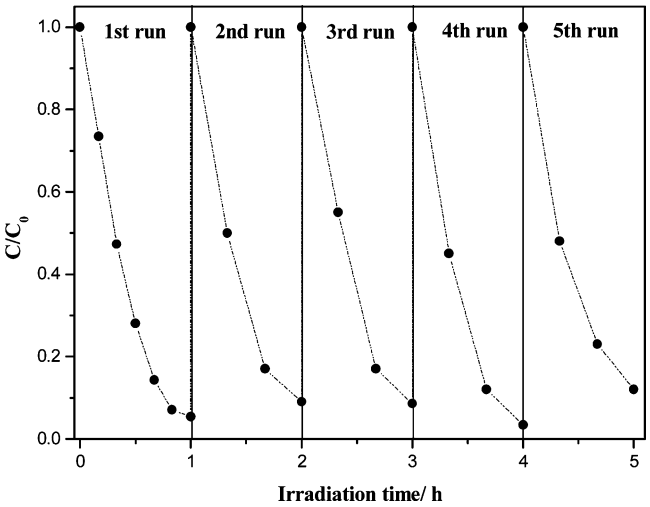

Figure 7. Cycling runs in the photocatalytic degradation of RhB in the presence of Bi_2WO_6 under visible-light irradiation; Bi_2WO_6 loading, 0.5 g L^{-1}; initial concentration of RhB, 1×10^{-5} M; $\lambda > 420$ nm; pH 7.5.

Therefore, the reaction of the photocatalytic degradation of RhB by Bi_2WO_6 is apparent first-order kinetics of the Langmuir−Hinshelwood model, whose apparent relationships are due to the low concentration of RhB chosen.

Bi_2WO_6 as a kind of heterogeneous photocatalyst can be easily recycled by a simple filtration because of its large density (9.505 g cm^{-3}). After five recycles for the photodegradation of RhB, the catalyst did not exhibit any significant loss of activity, as shown in Figure 7, confirming Bi_2WO_6 is not photocorroded during the photocatalytic oxidation of the pollutant molecules. XRD analysis of the sample also showed that the crystal structure of the photocatalyst was not changed after the photocatalytic reaction. The stability of a photocatalyst is important to its application; doped TiO_2 photocatalysts sometimes suffer from this problem.[25, 26]

3.2. Intermediates and Mineralized Degree. To identify the species produced in the photooxidation of RhB, the temporal proton NMR profiles of the dye, intermediates, and final products were monitored. Spectrum A in Figure 8 showed the typical proton NMR signals of pure RhB and their assignments to the various protons in the structure of RhB. The NMR signals of the aromatic hydrogens H_c, H_d, H_e, H_f, and H_g were located

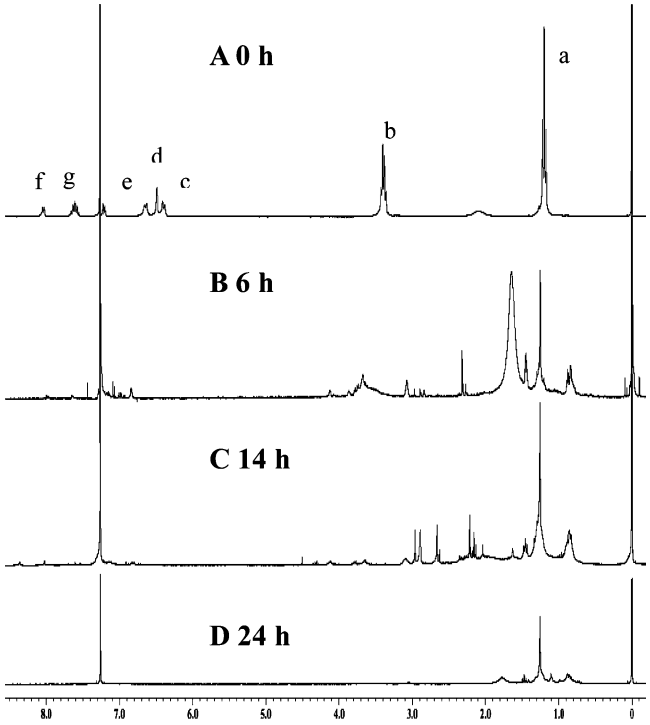

Figure 8. Temporal profile of the ^1H NMR spectra at various irradiation intervals during the photooxidation of RhB; initial concentration of RhB, 2×10^{-4} M; Bi_2WO_6 loading, 0.5 g L^{-1}, pH 7.50; $\lambda > 420$ nm.

at σ 6.66, 6.83−6.86, 6.96−6.99, 7.62−7.65, and 8.25−8.28 ppm, respectively; those of H_a and H_b of the *N*-diethyl group appeared at σ 1.18−1.23 and 3.40−3.60 ppm, respectively. During the course of the photocatalytic oxidation of RhB (spectra B−D in Figure 8), a series of new signals appeared at 1.23−1.40 ppm (hydrogens from CH_3 and analogous groups), 1.98, 3.00−3.20, and 7.00 ppm, whereas the characteristic signals of RhB at σ 1.18−1.23 (CH_3), 3.40−3.60 (CH_2), and 6.60−8.60 ppm (aromatic protons) disappeared. The intensity of the two new signals at σ 3.00−3.20 ppm increased with the increase of the irradiation time, while the methyl (CH_3) protons at σ 1.18−1.23 ppm and the methylene (CH_2) protons at σ 3.40−3.60 ppm of RhB decreased in intensity with the increase of the irradiation time. All of these indicated that N-demethylation and/or the destruction of the conjugated structure of RhB occurred in the suspensions during the course of irradiation.

The destruction of the RhB conjugated chromophore ring structure, decrease of TOC, and formation of NH_4^+ and NO_3^- in the photodegradation of RhB by Bi_2WO_6 was illustrated in Figure 9. The complete degradation of the dye required 20 h. The rate of TOC reduction was slower than that of the degradation of the dye; 29% of TOC still remained in the suspension after 20 h of irradiation when RhB was completely transformed. The mineralization yield reached a value of 92%. The decreasing rate of TOC exhibited two different behaviors before and after 18 h of irradiation, respectively, indicating that the mineralization of the dye goes through two different stages: the ring cleavage in the initial photocatalytic degradation stage and subsequent oxidation of the fragments in the latter stage. After 30 h of irradiation, the concentration of NH_4^+ rose to reach 55.0% (2.2×10^{-4} M) of the theoretical quantity (4.0×10^{-4} M). However, NO_3^- formation from the photooxidative step was insignificant, and less than ~7% of the stoichiometric nitrogen was found as NO_3^- after 30 h of irradiation. This showed that NH_4^+ is the main product of nitrogen transformation

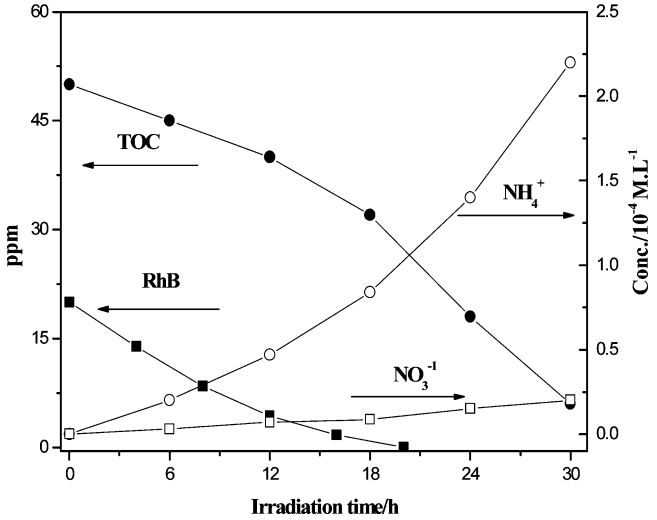

Figure 9. Changes in RhB concentration and TOC and the formation of NH_4^+ and NO_3^- during the course of photocatalytic degradation of RhB (2×10^{-4} M) in the presence of Bi_2WO_6 (0.5 g L^{-1}) at pH 7.50.

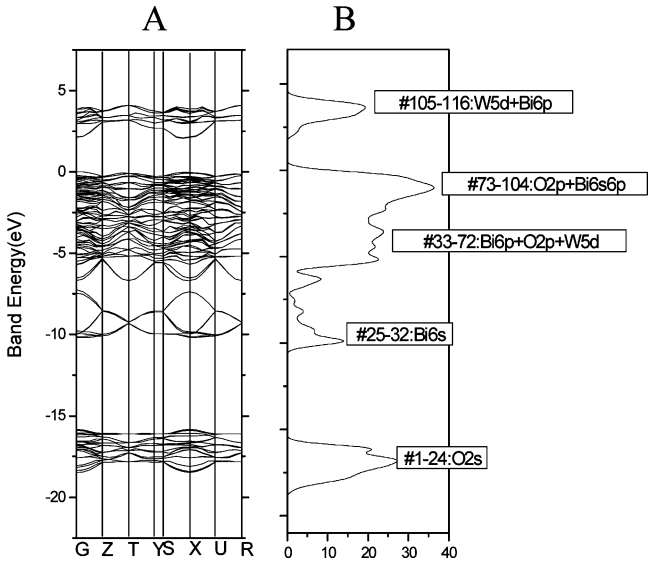

Figure 10. Energy band diagram (A) and density of states (B) for Bi_2WO_6 calculated by the DFT method.

for the photodegradation of RhB. Previous studies on the photocatalytic degradation of nitrogen-containing aromatics demonstrated that either photogenerated electrons and/or hydroxyl radicals act concurrently to transform the nitrogen-containing groups. The relative abundance of the main mineralization end-products (NH_4^+ and NO_3^-) largely depends on the initial oxidation state of nitrogen in the substituent group and on the substrate structure.[1,28,29]

3.3. Band Structure and Photoabsorption Properties. The energy level and the band gap of the oxide semiconductor will play a crucial role in determining its photocatalytic activity. In the present study, the electronic structure of Bi_2WO_6 was investigated by DFT calculations. The result is shown in Figure 10. The occupied bands of Bi_2WO_6 were classified into four bands. The lower-energy side in the occupied bands consisted of solely O2s (1−24#). The middle part of the occupied bands consisted of Bi6s orbitals (25−32#) and Bi6p+O2p+W5d hybrid orbitals (33−72#), respectively. The higher-energy side, that is, corresponding to the valence band (VB), consists of O2p+Bi6s hybrid orbitals (73−104#). The bottom of the conduction band (CB) was formed by the W5d orbitals, with a

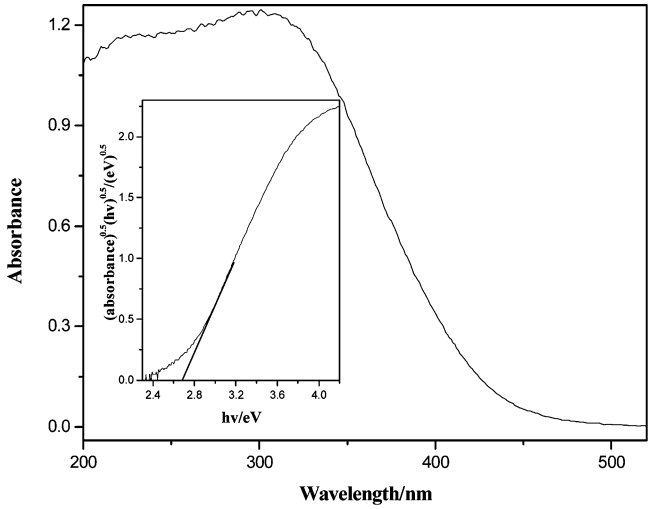

Figure 11. UV−visible diffuse reflectance spectra of bulk Bi_2WO_6 prepared by the hydrothermal synthesis in the present study.

small contribution of the Bi6p orbital. Thus, the highest occupied and lowest unoccupied molecular orbital levels were composed of the hybrid orbitals of O2p and Bi6s and the W5d orbitals, respectively. The band gap of Bi_2WO_6 is estimated to be 1.63 eV. Generally, the band gap calculated by DFT was smaller than that obtained experimentally, which is frequently pointed out as a common feature of DFT calculations.[29] The band structure indicates that charge transfer upon photoexcitation occurs from the O2p+Bi6s hybrid orbitals to the empty W5d orbitals. This transition which could be due to the 6s electrons usually occurs at a lower energy than the charge-transfer transition in WO_6^{6-}. The valence band of Bi_2WO_6 was composed of O2p and Bi6s, which is similar to that of $BiVO_4$. Zou et al.[9] have reported that the valence band of $CaBi_2O_4$ was attributed to the hybrid orbitals of O2p and Bi6s. All Bi-containing oxides may hold a similar valence band structure. The considerable visible-light absorption of Bi_2WO_6 is attributed to the transition from Bi6s to the W5d orbital.

It is well-known that light absorption by the material and the migration of the light-induced electrons and holes are the most key factors controlling a photocatalytic reaction, which is relevant to the electronic structure characteristics of the material.[9,10] The photoabsorption ability of the material was detected by UV−vis DRS, as shown in Figure 11. Bi_2WO_6 presented the photoabsorption properties from the UV light region to visible light shorter than 470 nm. The steep shape of the spectra indicated that the visible-light absorption was not due to the transition from the impurity level but was due to the band-gap transition. For a crystalline semiconductor, it was shown that the optical absorption near the band edge follows the equation[30] $ah\upsilon = A(h\upsilon - E_g)^n$, where a, υ, E_g, and A are the absorption coefficient, the light frequency, the band gap, and a constant, respectively. Among them, n decides the characteristics of the transition in a semiconductor. According to the equation, the value of n for Bi_2WO_6 was 1 from the data in Figure 11. The Bi ion charge in Bi_2WO_6 is +3. There are two 6s valence electrons of Bi in crystalline. The band gap of the photocatalyst was estimated to be 2.7 eV from the onset of the absorption edge. The color of the oxide was yellowish, as predicted from their photoabsorption spectrum.

3.4. Visible-Induced Degradation Mechanism. The photocatalytic oxidation of organic compounds is mainly considered to be controlled by the following processes:[10,31,32] (1) the photoabsorption of the semiconductor catalyst, (2) the generation

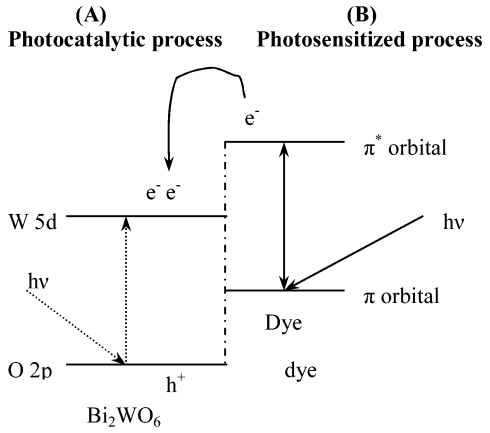

Figure 12. Possible pathway of the photoelectron transfer excited by visible-light irradiation, including process A (dotted line) and process b (solid line).

of photogenerated electron and hole, (3) the transfer of charge carriers, and (4) the utilization of the charge carriers by the reactants. Bi_2WO_6 exhibited the ability to absorb visible light, which is attributed to the transition of the electrons from the VB (the hybrid orbitals of O2p and Bi6s) to the CB (the W5d orbital) in the catalyst. It has been reported[22] that Bi_2WO_6 showed not only the activity for photocatalytic O_2 evolution but also the activity of mineralizing both $CHCl_3$ and CH_3CHO contaminants under visible-light irradiation. Therefore, the photocatalyst with a strong oxidizing potential could also be postulated. Furthermore, the hybridization of the Bi6s and O2p levels makes the VB largely dispersed, which favors the mobility of photoholes in the VB and is beneficial to the oxidation reaction.[9] Therefore, it is reasonable to believe Bi_2WO_6 is an active photocatalyst, and RhB could be degraded within a certain wavelength range of visible light over Bi_2WO_6. As shown in Figure 11, the light absorption by the oxides occurred dominantly when $\lambda < 470$ nm. Namely, RhB can be photocatalytically degraded when the wavelength is shorter than 470 nm (Figure 12A).

The photochemical experiment was also expanded to the other organic compound, 4-chlorophenol (4-CP). It is well-known that 4-CP has no light absorption characteristics in the visible spectral region (wavelengths longer than 400 nm). It was found that 4-CP was degraded efficiently by Bi_2WO_6 upon visible-light irradiation ($\lambda < 470$ nm) as RhB but in a longer irradiation time. Note that this photocatalytic method is not the color compound specific. Rather, Bi_2WO_6 is indeed a visible-light-induced photocatalyst.

In the present study, Bi_2WO_6 also showed the activity when the light wavelength was much longer than 470 nm, where it poorly absorbed the light radiation. About 19% of RhB was photodegraded after 60 min of irradiation ($\lambda > 490$ nm), as shown in Figure 13. It is well-known that RhB dye can absorb the visible light in the range 460−600 nm, which is attributed to the ground state and the excited state of the dye. Thus, the materials absorbing light irradiation should be RhB and Bi_2WO_6 together in the present work. Among them, RhB was the main material absorbing light irradiation when $\lambda > 470$ nm. When $\lambda > 470$ nm, the RhB photodegradation was attributed to the photosensitized mechanism. Namely, the RhB dye first absorbed the incident photon flux. Then, the photogenerated electrons were transferred to the excited state of the dye owing to the intramolecular $\pi-\pi^*$ transition and the dyes were oxidized. The photoelectrons of the excited state were immediately injected into the CB (W5d level) of Bi_2WO_6. The

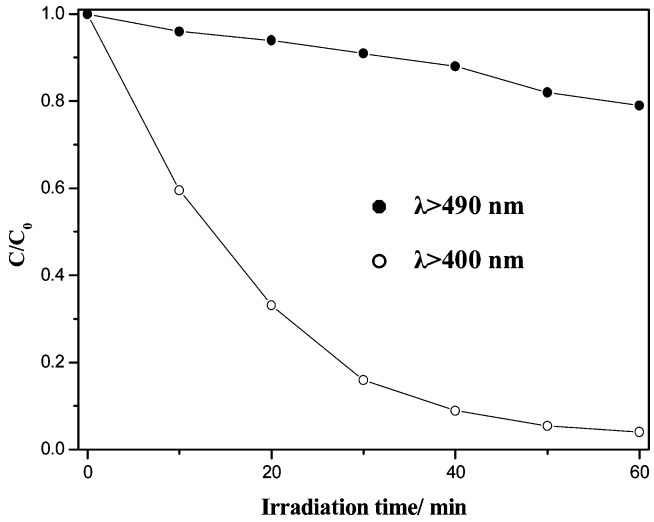

Figure 13. Photocatalytic degradation of RhB over Bi_2WO_6 particles under different irradiation lights; Bi_2WO_6 loading, 0.5 g L^{-1}; initial concentration of RhB, 1×10^{-5} M; pH 7.50.

photoelectrons in the CB were then captured by O_2, and the succeeding reactions can lead to the mineralization of the dyes. The photosensitized process is shown in Figure 12B. This process might be similar to the surface sensitization of TiO_2 via adsorbed dyes.[5,6] In this photochemical process, photosensitized degradation of dyes does not involve any VB hole; mineralization of dyes finds its origins with the active oxygen radical species, $O_2^{\bullet-}$, and the radical cations, $dye^{+\bullet}$. The reaction possibly includes the following:

$$RhB \rightarrow RhB^* \ (h\nu) \tag{3}$$

$$Bi_2WO_6 + RhB^* \rightarrow RhB^{\bullet+} + Bi_2WO_6(e) \tag{4}$$

$$Bi_2WO_6(e) + O_2 \rightarrow Bi_2WO_6 + O_2^{\bullet-} \tag{5}$$

$$RhB^{\bullet+} + O_2/O_2^{\bullet-} \rightarrow \text{intermediate product} \tag{6}$$

Both the photocatalytic process and the photosensitized process would work concurrently when the light wavelength was longer than 420 nm, but the former is the predominant process, which could be concluded from Figure 13. The reaction rate of RhB photodegradation initiated by the light-excited dye was much slower than that initiated by the light-excited Bi_2WO_6. As mentioned above, only 19% of RhB was transformed by photosensitized action. The photosensitized process worked solely when the light wavelength was longer than 470 nm.

3.5. Involved Active Species and the Role of Oxygen. The RhB/Bi_2WO_6 system was examined by DMPO spin-trapped ESR spectroscopy to monitor the active radicals that form during the photodegraded process. For comparison, the RhB/TiO_2 system was also observed under the same conditions. The results are summarized in Figure 14. There were no signals when the RhB/Bi_2WO_6 suspension was irradiated. However, in the case of RhB/TiO_2, a spectrum displaying signals with characteristic intensity 1:2:2:1 for DMPO−•OH adducts was obtained, indicating that the •OH radical was formed.[33−35] In another experiment, it was found that the addition of 2-propanol, a well-known scavenger of •OH radicals,[36] into the photoreaction system did not cause the apparent changes in the degradation rate of RhB, as shown in Figure 15. This indicates that the free •OH radicals could not be the main active oxygen species in this photochemical process.

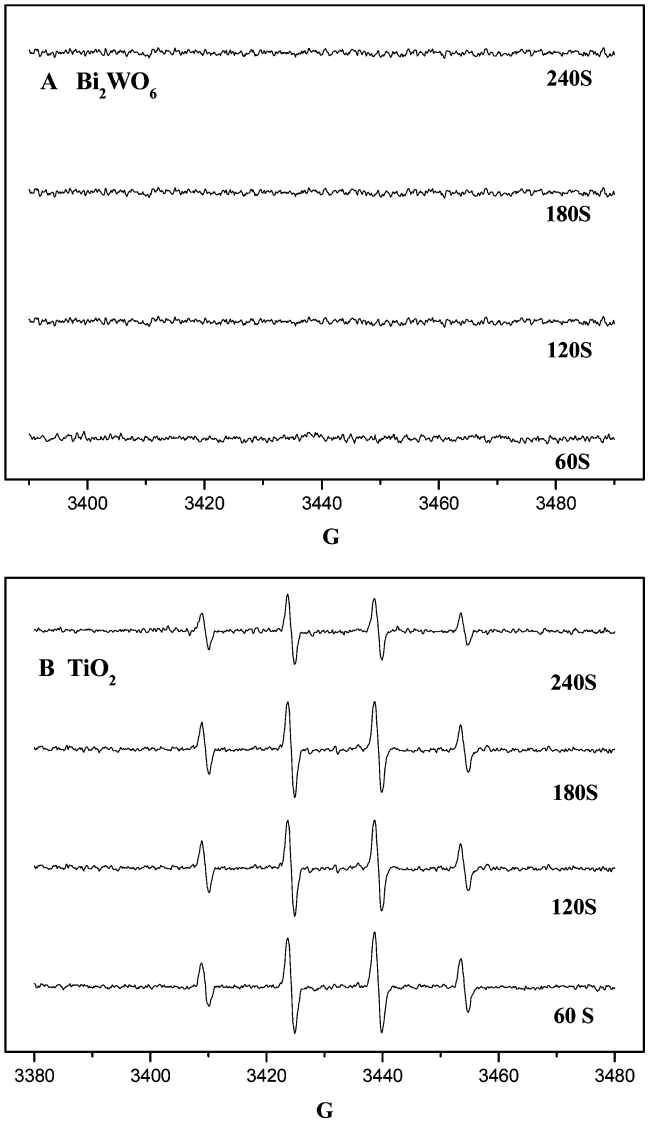

Figure 14. ESR signals of the DMPO−•OH adducts as a function of light illumination time. DMPO (0.15 M), $\lambda = 355$ nm; A, 0.5 g $L^{-1}Bi_2WO_6$, pH 7.50, RhB, 5×10^{-5} M; B, 0.5 g L^{-1} TiO_2, pH 4.50, RhB, 5×10^{-5} M.

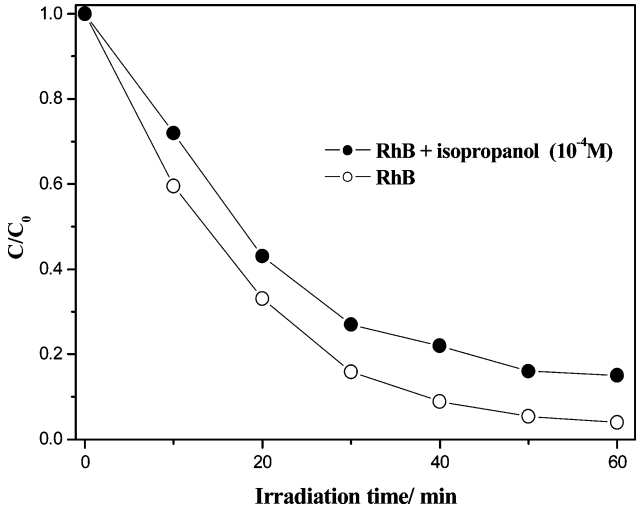

Figure 15. Photocatalytic degradation of RhB over Bi_2WO_6 particles under different solutions; Bi_2WO_6 loading, 0.5 g L^{-1}; initial concentration of RhB, 1×10^{-5} M; pH 7.50.

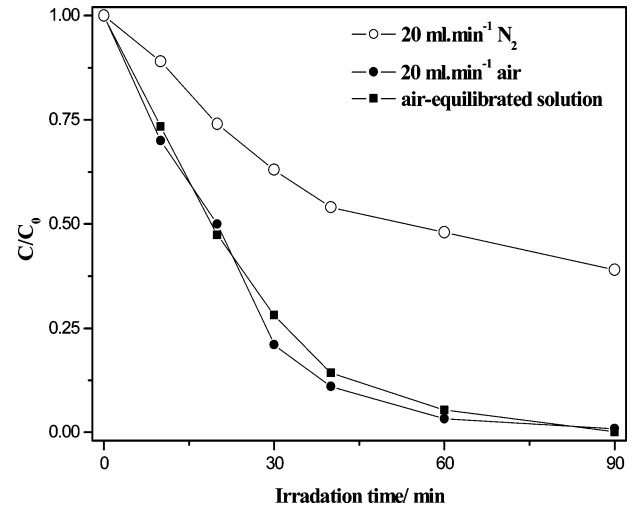

Figure 16. Photocatalytic degradation of RhB over Bi_2WO_6 particles in N_2-saturated, air-saturated, or air-equilbrated solutions; Bi_2WO_6 loading, 0.5 g L^{-1}; initial concentration of RhB, 1×10^{-5} M; $\lambda > 420$ nm; pH 7.50.

From the theoretical viewpoint, the production of •OH in the present system is almost impossible. Generally, in a valence band formed by Bi^{3+}, holes formed by photoexcitation are regarded as Bi^{5+} (or Bi^{4+}). Although a redox potential in an aqueous solution is different from that in solids, a standard redox potential of Bi_2O_4/BiO^+ (Bi^{V}/Bi^{III}) ($E° = +1.59$ V at pH 0) could make sense for a rough estimation of the oxidation potential of hole (Bi^{5+}) photogenerated in the Bi_2WO_6 photocatalyst.[37] However, the standard redox potential of Bi^{V}/Bi^{III} is more negative than that of $OH•/OH^-$ (+1.99),[38] suggesting that the hole photogenerated on the surface of Bi_2WO_6 could not react with OH^-/H_2O to form •OH. Therefore, the decomposition of RhB by Bi_2WO_6 could be due to the reaction with the photogenerated hole directly. Following the general information, we have reason to assume that the degradation of RhB on Bi_2WO_6 is not the involvement of •OH radicals. The direct hole transfer could play an important role. As a result, the photodegradation of RhB on Bi_2WO_6 is little affected by the presence of the •OH radical scavenger.

As mentioned above, the photosensitized process would work concurrently when the light wavelength was longer than 420 nm. Therefore, it could be postulated that $O_2^{\bullet-}$ is the other pivotal active species for Bi_2WO_6 photocatalysis. It is worth noting that the generation of $O_2^{\bullet-}$ could be via two competitive processes. On one hand, RhB (as a photosensitizer) is excited by visible light; the excited dye then injects an electron into the CB of the catalyst via electron transfer to generate a conduction electron that is scavenged by the adsorbed O_2 on the surface of the catalyst to form $O_2^{\bullet-}$. Once the dispersion discolors completely, the formation of $O_2^{\bullet-}$ by this route will terminate automatically; on the other hand, when the catalyst absorbs light, the formation of $O_2^{\bullet-}$ could be by the photogenerated electron reacting directly with O_2 adsorbed on the surface of the catalyst. The production of $O_2^{\bullet-}$ carries through the whole photochemical process.

To understand the effect of oxygen, the photocatalytic reactivity in the presence of dissolved oxygen should be compared with the anoxic reactivity. RhB photolysis could be carried out with continuous N_2-sparging and thus in a stricter anoxic condition because RhB was nonvolatile. The result is shown in Figure 16. Under the anoxic suspension, the photodegraded rate of RhB was largely prohibited. Apparently, the presence of oxygen is responsible for the significant reduction. The presence of oxygen is important, and its effect is to

primarily act as an efficient e^- trap, leading to the generation of $O_2^{\bullet-}$ and preventing the recombination of e^- and h^+. In the suspension of continued air-purged, the relatively small difference could be observed, compared to that in the air-equilibrated solution. This is not surprising in view of there being enough oxygen for the photodegradation of RhB under the experimental conditions used.

4. Conclusions

Visible-light-induced degradation of RhB over the nanosized Bi_2WO_6 was observed. Bi_2WO_6 exhibited a high activity for the RhB degradation. The relative high-mineralized degree of RhB was also achieved. The Bi_2WO_6-assisted photodegradation of RhB occurs via two competitive processes: a photocatalytic process and a photosensitized process. RhB degradation occurs mainly via the photocatalytic process. Kinetic studies by using ESR and the radical scavenger technologies suggest that •OH is not the dominant photooxidant. Direct hole transfers and $O_2^{\bullet-}$ could take part in Bi_2WO_6 photocatalysis.

Development of Bi_2WO_6-based photocatalytic technologies requires proper understanding of their characteristics. The detailed kinetics and mechanisms in this work should provide valuable knowledge in this respect. This system possesses several advantages: (i) the strong photooxidative ability to directly degrade the dye pollutants, (ii) the relative high-mineralized degree could be expected, (iii) the mild reaction conditions including the biocompatible pH values. All of these suggest that the idea of using Bi_2WO_6 could be a plausible strategy to develop an efficient visible-light-driven photocatalyst for the destruction of the dye pollutants.

Acknowledgment. The authors appreciate Chinese National Science Foundation (20433010), Trans-Century Training Program Foundation for the Talents by the Ministry of Education, P. R. C., and the Excellent Young Teacher Program of MOE, P. R. China, for financial support.

Supporting Information Available: Figures showing photocatalytic degradation of 4-CP, XPS of *N*-doped TiO_2, and photocatalytic photodegradation of RhB. This material is available free of charge via the Internet at http://pubs.acs.org.

References and Notes

(1) Horikoshi, S.; Hojo, F.; Hikaka, H.; Serpone, N. *Environ. Sci. Technol.* **2004**, *38*, 2198.
(2) Xu, Y. M.; Langfor, C. H. *Langmuir* **2001**, *17*, 897.
(3) Bao, N.; Feng, X.; Yang, Z.; Shen, L.; Lu, X. *Environ. Sci. Technol.* **2004**, *38*, 2729.
(4) Vinodgopal, K.; Wynkoop, D. E. *Environ. Sci. Technol.* **1996**, *30*, 1660.
(5) Chen, C.; Zhao, W.; Li, J.; Zhao, J. *Environ. Sci. Technol.* **2002**, *36*, 3604.
(6) Huang, Y.; Li, J.; Ma, W.; Cheng, M.; Zhao, J. *J. Phys. Chem. B* **2004**, *108*, 7263.
(7) Chen, C.; Zhao, W.; Lei, P.; Zhao, J.; Serpone, N. *Chem. Eur. J.* **2004**, *10*, 1956.
(8) Zou, Z.; Ye, J.; Sayama, K.; Arakawa, H. *Nature* **2001**, *414*, 625.
(9) Tang, J.; Zou, Z.; Ye, J. *Angew. Chem., Int. Ed.* **2004**, *43*, 4463.
(10) Tang, J.; Zou, Z.; Ye, J. *Chem. Mater.* **2004**, *16*, 1644.
(11) Abe, R.; Higashi, M.; Zou, Z.; Sayama, K.; Abe, Y.; Arakawa, H. *J. Phys. Chem. B* **2004**, *108*, 811.
(12) Zou, Z.; Ye, J.; Arakawa, H. *J. Phys. Chem. B* **2002**, *106*, 13098.
(13) Kudo, A.; Omore, K.; Kato, H. *J. Am. Chem. Soc.* **1999**, *121*, 11459.
(14) Tokunaga, S.; Kato, H.; Kudo, A. *Chem. Mater.* **2001**, *13*, 4624.
(15) Kohtani, S.; Hiro, J.; Yamamoto, N. *Catal. Commun.* **2005**, *6*, 185.
(16) Kudo, A.; Ueda, K.; Kato, H. *Catal. Lett.* **1998**, *53*, 229.
(17) Yao, W.; Wang, H.; Xu, X.; Zhou, J.; Yang, X.; Zhang, Y.; Shang, S. *Appl. Catal., A* **2004**, *259*, 29.
(18) Yao, W.; Xu, X.; Wang, H.; Zhou, J.; Yang, X.; Shang, S.; Huang, B. *Appl. Catal., B* **2004**, *52*, 109.
(19) Shi, Y.; Feng, S.; Cao, C. *Mater. Lett.* **2000**, *44*, 215.
(20) Kudo, A.; Hijii, S. *Chem. Lett.* **1999**, 1103.
(21) Tang, J.; Zou, Z.; Ye, J. *Catal. Lett.* **2004**, *92*, 53.
(22) Zhang, C.; Zhu, Y. *Chem. Mater.* **2005**, *17*, 3537.
(23) Kohn, W.; Sham, L. *Phys. Rev. A* **1965**, *140*, 1133.
(24) Perdew, J. P.; Wang, W. *Phys. Rev. B* **1992**, *45*, 13244.
(25) Bae, E.; Choi, W. *Environ. Sci. Technol.* **2003**, *37*, 147.
(26) He, J. J.; Hagfeldt, A.; Lindquist, S. E. *Langmuir* **2001**, *17*, 2743.
(27) Choi, W.; Kim, S. *Environ. Sci. Technol.* **2002**, *36*, 2019.
(28) Wu, T.; Liu, G.; Zhao, J.; Hidaka, H.; Serpone, N. *New J. Chem.* **2000**, *24*, 93.
(29) Dreizler, R. M.; Gross, E. K. *Density Functional Theory: An Approach to the Quantum Many-Body Problem*; Springer-Verlag: Berlin, 1990.
(30) Butler, M. A. *Appl. Phys.* **1977**, *48*, 1914.
(31) Nagaveni, K.; Sivalingam, G.; Hegde, M. S.; Madras, G. *Environ. Sci. Technol.* **2004**, *38*, 1600.
(32) Wong, C. C.; Chu, W. *Environ. Sci. Technol.* **2003**, *37*, 2310.
(33) Li, X.; Liu, G.; Zhao, J. *New J. Chem.* **1999**, *23*, 1193.
(34) Chen, C.; Li, X.; Ma, W.; Zhao, J. *J. Phys. Chem. B* **2002**, *106*, 318.
(35) Wu, T.; Lin, T. Zhao, J. *Environ. Sci. Technol.* **1999**, *33*, 1379.
(36) Li, J.; Ma, W.; Huang, Y.; Tao, X.; Zhao, J.; Xu, Y. *Appl. Catal., B* **2004**, *48*, 17.
(37) Weast, R. C.; *Handbook of Chemistry and Physics*; CRC Press: Boca Raton, FL, 1988.
(38) Kim, S.; Choi, W. *Environ. Sci. Technol.* **2002**, *36*, 2019.